Instantaneous Gearshift Model Based on Gear-dependent Angular Momentum

Davide Tebaldi *, **Roberto Zanasi** **

* DIEF, Department of Engineering "Enzo Ferrari"
University of Modena and Reggio Emilia, Modena, Italy
(e-mail: davide.tebaldi@unimore.it).
** DIEF, Department of Engineering "Enzo Ferrari"
University of Modena and Reggio Emilia, Modena, Italy
(e-mail: roberto.zanasi@unimore.it).

Abstract: The paper presents a new gearbox dynamic model for the effective simulation of simultaneous multi-clutches lock/unlock, by exploiting the Power-Oriented Graphs (POG) modeling technique. The generalized structure of the proposed model allows to simulate various gearbox configurations, which may foresee a change in terms of equivalent moment of inertia on the primary or secondary shaft, depending on the internal clutches configuration being function of the currently engaged gear. The peculiarity of the model lies in the instantaneous engagement of the new gear by skipping the slipping transient related to change of the internal clutches configuration, while preserving the natural loss of energy associated to it. The effectiveness of the presented gearbox model is finally tested and compared with classical gearbox modeling solutions with the aid of some simulation results.

Keywords: Dynamic modelling, Models, Model reduction, Model-based control, Automotive control, System models, Real-time systems, Execution times.

1. INTRODUCTION

The promotion of model-based approaches is more and more widespread in all the companies working in the automotive and agricultural fields, with the purpose of simulating entire parts of the vehicle on dedicated platforms so as to investigate and test the system dynamics. A good trade-off between the level of details to be included in the model and the computational complexity must always be subject of a careful evaluation, in order to make the model as suitable for the analyzed application as possible.

In model-based approaches, particular attention has to be paid to fast dynamics, from which troubles may arise since the real-time execution of such models requires to perform fixed step size simulations. When dealing with hybrid or traditional propulsion systems, a physical element which is certainly critical from a simulative point of view is the gearbox, which is responsible for the engagement/disengagement of several gears according to the control strategy for properly driving the vehicle transmission system. Depending on the currently engaged gear, the gearbox configuration undergoes some changes according to the lock/unlock of the internal clutches so as to guarantee the proper velocity and torque ratios. Typically, the gearshift also implies a change in terms of equivalent moment of inertia rigidly connected to the primary or secondary shafts, as a function of the gearbox internal gears configuration.

The starting point for modeling complex gearboxes is the correct modeling of a single clutch, allowing to couple/decouple two plates. Several papers are present in the literature concerning the dynamic modeling of the lock, unlock and slipping phases of clutches, see Lhomme et al. (2007), SUN et al. (2008), Zoppi et al. (2013) and Bachinger et al. (2014), mainly relying on the introduction of a proper Coulomb friction torque acting on both plates of the clutch multiplied by the proper gear radius. In Zanasi et al. (2001) and Grossi and Zanasi (2015), the authors model the presence of the Coulomb friction acting on the two clutch plates through a "sign" function, applied to the difference of the two plates velocities and multiplied by a proper factor. This represents an easy and effective modeling solution, which is correct from an energetic point of view as the expected energy loss takes place. However, this approach presents the following drawback: when the two plates velocities become equal each other after the transient, function "sign" gives rise to an oscillation at very high frequency, which may cause trouble in fixed step size simulations for real-time applications.

The solution proposed in this paper, which exploits the POG modeling technique (see Zanasi (2010)), does not require the usage of a Coulomb friction torque or any other coupling action to simulate the clutch slipping phase, in which the transient involving the two clutch plates occurs. In fact, the new velocities of the two plates after the transient are computed by exploiting a properly defined angular momentum and the slipping phase is no longer present, making the proposed solution very effective from a simulative point of view. Instantaneous gearshift can therefore take place, ensuring the same energy loss associated to gear shifting as standard modeling solutions.

This paper is organized as follows: in Sec. 2, the instantaneous gearbox model is presented for the case of
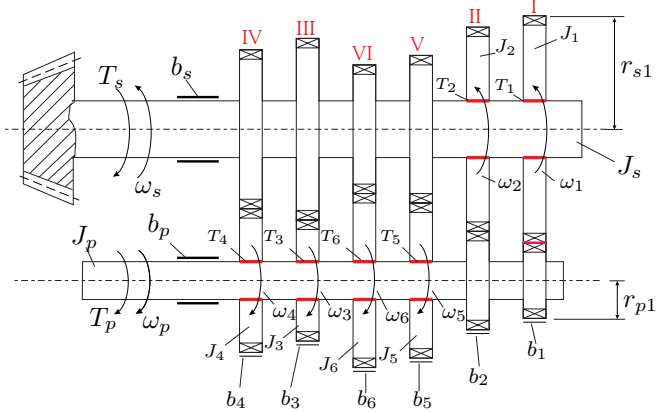
Fig. 1. Schematic representation of a six gearbox system.

one-dimensional dynamics on the gearbox primary and secondary and employed to model a six gearbox system as a case study. A comparison between the simulation results given by a "classical" modeling approach and those given by the proposed solution is then made. In Sec. 3, the proposed model for instantaneous gear shifting is extended to the multidimensional case and tested in simulation with reference to a new case study. The latter is composed of the same gearbox as the one in Sec. 2 by connecting the primary shaft to a planetary gear, whose model is given in Sec. 3.1 with reference to Zanasi and Grossi (2009) and Zanasi and Tebaldi (2019), thus making the primary dynamics two-dimensional. Finally, Sec. 4 provides the conclusions of this work.

2. CASE STUDY: A SIX GEARBOX SYSTEM

A schematic representation of the considered six gearbox system is shown in Fig. 1. The red lines shown in Fig. 1 are the points where the gearbox actual clutches act in order to engage the desired gear: in the considered gearbox, only one clutch is "on" and active at a time, while all the others are "off". Parameters T_p, ω_p, J_p and b_p are the external torque, the angular velocity, the moment of inertia and the angular viscous friction coefficient of the primary shaft. Parameters T_s, ω_s, J_s and b_s have analogous meanings related to the secondary shaft variables; r_{p1}, r_{p2}, ..., r_{p6} are the radii of the gear wheels connected to the primary shaft and r_{s1}, r_{s2}, ..., r_{s6} are the radii of the gear wheels connected to the secondary shaft. Angular velocities ω_1 and ω_2 are those of the gear wheels having moment of inertia J_1 and J_2, respectively, around the secondary shaft; whereas angular velocities ω_3, ω_4, ω_5 and ω_6 are those of the gear wheels having moment of inertia J_3, J_4, J_5 and J_6, respectively, around the primary shaft. Variables T_1, T_2, ..., T_6 are the maximum values of the Coulomb friction torques present between the j-th idle gear wheel, for $j \in [1, 2, \ldots, 6]$, and the shaft on which the j-th idle gear wheel itself is mounted. These torques are used in the gearbox to engage the desired gear.

2.1 Gearbox system: full dynamic model

The POG full dynamic model of the gearbox system in Fig. 1 is shown in Fig. 2, see Zanasi et al. (2002). Vectors $\mathbf{r}_p$ and $\mathbf{r}_s$ are defined as follows:
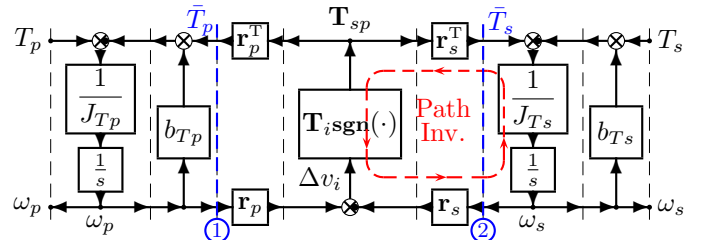

Fig. 2. POG full dynamic model of the system in Fig. 1.

$$\mathbf{r}_p = \begin{bmatrix} 1/\alpha_{sp1} \\ 1/\alpha_{sp2} \\ 1 \\ 1 \\ 1 \\ 1 \end{bmatrix}, \quad \mathbf{r}_s = \begin{bmatrix} 1 \\ 1 \\ \alpha_{sp3} \\ \alpha_{sp4} \\ \alpha_{sp5} \\ \alpha_{sp6} \end{bmatrix}, \quad \alpha_{spj} = \frac{r_{sj}}{r_{pj}} = \frac{\omega_{pj}}{\omega_{sj}}$$

$$\text{for } j \in [1, 2, \ldots, 6].$$

Parameters r_{pj} and r_{sj} are the medium radii of the j-th gear wheels mounted on the primary and secondary shafts, respectively. Variables ω_{pj} and ω_{sj} are the angular velocities of the primary and secondary shafts when the j-th gear is engaged. The definition of vector $\mathbf{T}_i \, \mathbf{sgn}(\cdot)$ present in the POG scheme of Fig. 2 is the following:

$$\mathbf{T}_i \mathbf{sgn}(\cdot) = \begin{bmatrix} T_1(i)\,\text{sgn}(\Delta v_1) \\ T_2(i)\,\text{sgn}(\Delta v_2) \\ T_3(i)\,\text{sgn}(\Delta v_3) \\ T_4(i)\,\text{sgn}(\Delta v_4) \\ T_5(i)\,\text{sgn}(\Delta v_5) \\ T_6(i)\,\text{sgn}(\Delta v_6) \end{bmatrix}, \quad T_j(i) = \begin{cases} T_i & \text{if } i = j \\ 0 & \text{if } i \neq j \end{cases} \quad (1)$$

$$\Delta v_i = r_{pi}\,\omega_p - r_{si}\,\omega_s.$$

Additionally, parameters α_{psj} are defined as follows:

$$\alpha_{psj} = \frac{1}{\alpha_{spj}} = \frac{r_{pj}}{r_{sj}} = \frac{\omega_{sj}}{\omega_{pj}}, \quad \text{for } j \in [1, 2, \ldots, 6]. \quad (2)$$

The expressions of moments of inertia J_{Tp} and J_{Ts} are:

$$J_{Tp} = J_p + J_1\alpha_{ps1}^2 + J_2\alpha_{ps2}^2$$

$$J_{Ts} = J_s + J_3\alpha_{sp3}^2 + J_4\alpha_{sp4}^2 + J_5\alpha_{sp5}^2 + J_6\alpha_{sp6}^2$$

Linear friction coefficients b_{Tp} and b_{Ts} are given by:

$$b_{Tp} = b_p + b_1\alpha_{ps1}^2 + b_2\alpha_{ps2}^2$$

$$b_{Ts} = b_s + b_3\alpha_{sp3}^2 + b_4\alpha_{sp4}^2 + b_5\alpha_{sp5}^2 + b_6\alpha_{sp6}^2.$$

2.2 Gearbox system: reduced dynamic model

According to the definition of vector $\mathbf{T}_i \, \mathbf{sgn}(\cdot)$ given in (1), the torques $\bar{T}_p$ and $\bar{T}_s$ in power sections ① and ② in Fig. 2 can be considered as "scalar", because only one element of vector $\mathbf{T}_i \, \mathbf{sgn}(\cdot)$ is different from zero at a time. This means that, by considering the model at a certain time instant, vectors $\mathbf{r}_p$, $\mathbf{r}_s$ and $\mathbf{T}_{sp}$ can be assumed to be "scalar" as well, where the nonzero elements are radii r_{pj}, r_{sj} and $T_{sp} = T_j \text{sgn}(\Delta v_j)$, respectively. Using this observation, a path inversion can be applied to the full POG block scheme of the gearbox, as highlighted by the red dashed line in Fig. 2. Along the inverted path, the quantity Δv_i is equal to zero when the gear is engaged and is different from zero during the synchronization phase only, i.e. during the transient. By applying the path inversion depicted in red in Fig. 2, and neglecting the inverse of $\mathbf{T}_i \, \mathbf{sgn}(\cdot)$ when the gear is engaged, one obtains the POG reduced dynamic model of the considered gearbox system shown in Fig. 3. One can easily verify that
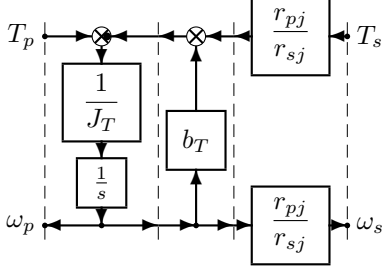
Fig. 3. POG reduced dynamic model of system in Fig. 1.

the moment of inertia J_T and the viscous linear friction coefficient b_T have the following expressions:

$$J_T = J_{T_p} + J_{T_s}\left(\frac{r_{pj}}{r_{sj}}\right)^2 \qquad b_T = b_{T_p} + b_{T_s}\left(\frac{r_{pj}}{r_{sj}}\right)^2 \quad (3)$$

The new simplified block scheme in Fig. 3 is characterized by the following angular momentum $Q_{Gp}(j)$:

$$Q_{Gp}(j) = J_{T_p}\omega_p + \alpha_{psj}J_{Ts}\omega_s \qquad (4)$$

which is a function of the engaged gear j.

Property 1. By neglecting the friction coefficient b_T and assuming that the system input torques are $T_p = T_s = 0$, the angular momentum $Q_{Gp}(j)$ remains constant also during the clutch synchronization phases, as long as j is constant.

Proof. The proof is given assuming that the friction torque T_{sp} is a generic function of time $T_{sp} = T_{sp}(t)$. Using (2), the angular momentum in (4) becomes:

$$Q_{Gp}(j) = J_{Tp}\omega_p + \frac{r_{pj}}{r_{sj}}J_{Ts}\omega_s \qquad (5)$$

Since b_T is in general very small, it can be assumed to be equal to zero, i.e. $b_{T_p} = b_{T_s} = 0$ from (3). By making this assumption and assuming zero input torques, $T_p = T_s = 0$, one can explicitly write the angular velocities ω_p and ω_s from the full POG block scheme in Fig. 2 as follows:

$$\omega_p = \int\left(\frac{-\bar{T}_p}{J_{T_p}}\right)dt = \int\underbrace{\left(\frac{-T_{sp}(t)\,r_{pj}}{J_{T_p}}\right)}_{f_1(t)}dt$$

$$\omega_s = \int\left(\frac{\bar{T}_s}{J_{T_s}}\right)dt = \int\underbrace{\left(\frac{T_{sp}(t)\,r_{sj}}{J_{T_s}}\right)}_{f_2(t)}dt \qquad (6)$$

Using (6), momentum $Q_{G_P}(j)$ in (5) can be rewritten as:

$$Q_{Gp}(j) = J_{Tp}\int\left(\frac{-T_{sp}(t)\,r_{pj}}{J_{T_p}}\right)dt + \frac{r_{pj}}{r_{sj}}J_{Ts}\int\left(\frac{T_{sp}(t)\,r_{sj}}{J_{T_s}}\right)dt$$

By solving the previous equation, one obtains:

$$Q_{Gp}(j) = J_{Tp}\underbrace{\left[\frac{-\bar{T}_{sp}(t)\,r_{pj}}{J_{T_p}} + C_1\right]}_{F_1(t)} + \frac{r_{pj}}{r_{sj}}J_{Ts}\underbrace{\left[\frac{\bar{T}_{sp}(t)\,r_{sj}}{J_{T_s}} + C_2\right]}_{F_2(t)} \quad (7)$$

where $\bar{T}_{sp}(t) = \int_0^t T_{sp}(t)\,dt$ is a particular primitive of function $T_{sp}(t)$, C_1 and C_2 are the two integration constants, and $F_1(t)$ and $F_2(t)$ describe the family of primitive functions associated to $f_1(t)$ and $f_2(t)$ introduced in (6). By doing some algebra on (7), one obtains:

$$Q_{Gp}(j) = J_{T_p}C_1 + \frac{r_{pj}}{r_{sj}}J_{Ts}C_2 \qquad (8)$$

Since C_1 and C_2 are constant according to the definition of family of primitive functions, and J_{T_p}, J_{T_s}, r_{pj} and r_{sj}

are constant as long as j is constant, i.e. the assumption made in Prop. 1, it follows that Eq. (8) is constant. □

Let t_{ij} be the instant at which the gearbox is switched from gear i to gear j. If gear i is fully engaged at instant t_{ij}^-, the angular velocity $\omega_s(t_{ij})$ of the secondary shaft at instant t_{ij} can be expressed as follows:

$$\omega_s(t_{ij}) = \alpha_{psi}\,\omega_p(t_{ij}). \qquad (9)$$

At instant t_{ij}^+, i.e. when the new gear j starts to be engaged, the new value of the angular momentum $Q_{Gp}(j, t_{ij}^+)$ given in (4) at instant t_{ij}^+ can be expressed as follows:

$$\begin{aligned}Q_{Gp}(j, t_{ij}^+) &= J_{Tp}\,\omega_p(t_{ij}^+) + \alpha_{psj}J_{Ts}\,\omega_s(t_{ij}^+)\\ &= (J_{Tp} + \alpha_{psj}J_{Ts}\,\alpha_{psi})\omega_p(t_{ij})\end{aligned} \qquad (10)$$

where the last expression has been obtained using (9) and equalities $\omega_p(t_{ij}^+) = \omega_p(t_{ij})$, $\omega_s(t_{ij}^+) = \omega_s(t_{ij})$, which hold as the new gear has just been engaged at instant $t = t_{ij}^+$.

For $t > t_{ij}$, angular momentum $Q_{Gp}(j, t)$ remains constant:

$$Q_{Gp}(j, t) = J_{Tp}\,\omega_p(t) + \alpha_{psj}J_{Ts}\,\omega_s(t) = Q_{Gp}(j, t_{ij}^+) \quad (11)$$

and equal to the value $Q_{Gp}(j, t_{ij}^+)$ given in (10) until a new gear engagement occurs. At time instant t_j, with $t_j > t_{ij}$, when the new gear j is fully engaged (i.e. transient ended), the angular velocities ω_p and ω_s are related as follows:

$$\omega_s(t_j) = \alpha_{psj}\,\omega_p(t_j)$$

and the angular momentum $Q_{Gp}(j, t_j)$ is given by:

$$\begin{aligned}Q_{Gp}(j, t_j) &= J_{Tp}\,\omega_p(t_j) + \alpha_{psj}J_{Ts}\,\omega_s(t_j)\\ &= (J_{Tp} + \alpha_{psj}J_{Ts}\,\alpha_{psj})\omega_p(t_j) = Q_{Gp}(j, t_{ij}^+)\end{aligned} \qquad (12)$$

From (10) and (12), the value of the angular velocity $\omega_p(t_j)$ of the primary shaft at time t_j can be determined:

$$\omega_p(t_j) = \frac{(J_{Tp} + \alpha_{psj}J_{Ts}\,\alpha_{psi})}{(J_{Tp} + \alpha_{psj}J_{Ts}\,\alpha_{psj})}\omega_p(t_{ij}) \qquad (13)$$

Relation (13) gives the angular velocity $\omega_p(t_j)$ of the primary shaft at time instant t_j, that is when the synchronization phase ends and the new gear j is fully engaged.

The POG reduced dynamic model of the gearbox reported in Fig. 3 exploits relation (13) to properly reset the integrator with the new initial condition any time a gearshift occurs, thus skipping the system transient.

2.3 Gearbox system: simulation

In this section, the system in Fig. 1 is simulated using the full and reduced gearbox models in Fig. 2 and Fig. 3, respectively, to compare the results. The simulations last for $T_{fin} = 1.1$ [s] and the initial angular velocities of the primary and secondary shafts are $\omega_{p_0} = 3000$ [rpm] and $\omega_{s_0} = \alpha_{ps1}\omega_{p_0} = 912.96$ [rpm]. The system parameters values are reported in Table 1, whereas Fig. 4 shows the engaged gear vs time. The simulations results are shown in Fig. 5 and Fig. 6. The left subplot of Fig. 5 shows the primary shaft velocity ω_p (continuous lines) and the secondary shaft velocity ω_s (dashed lines) vs time for the simulation performed on the full gearbox model (magenta lines) and for the simulation performed on the reduced gearbox model (blue lines). The right subplot of Fig. 5 shows the reduction ratio α_{spj} vs time for the full gearbox model (magenta line) and for the reduced

Table 1. Parameters for simulation in Sec. 2.3.

α_{sp1}	3.286	J_1	0.00465 $[\mathrm{kg\,m^2}]$
α_{sp2}	2.158	J_2	0.00333 $[\mathrm{kg\,m^2}]$
α_{sp3}	1.609	J_3	0.00073 $[\mathrm{kg\,m^2}]$
α_{sp4}	1.269	J_4	0.00131 $[\mathrm{kg\,m^2}]$
α_{sp5}	1.034	J_5	0.00183 $[\mathrm{kg\,m^2}]$
α_{sp6}	0.848	J_6	0.00242 $[\mathrm{kg\,m^2}]$
J_p	0.0195 $[\mathrm{kg\,m^2}]$	b_p, b_s, b_j	0 $[\mathrm{Nm\,s\,/\,rad}]$
J_s	0.0768 $[\mathrm{kg\,m^2}]$	T_j	40 $[\mathrm{Nm}]$
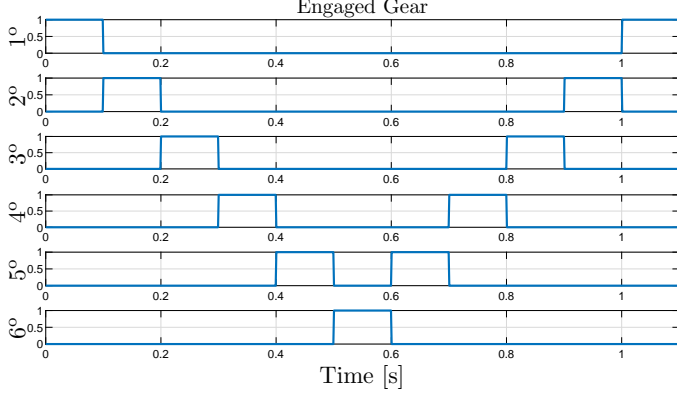
Fig. 4. Engaged gear as a function of time.
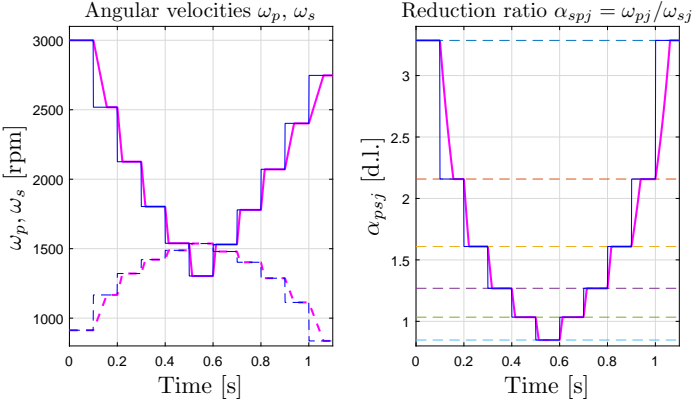
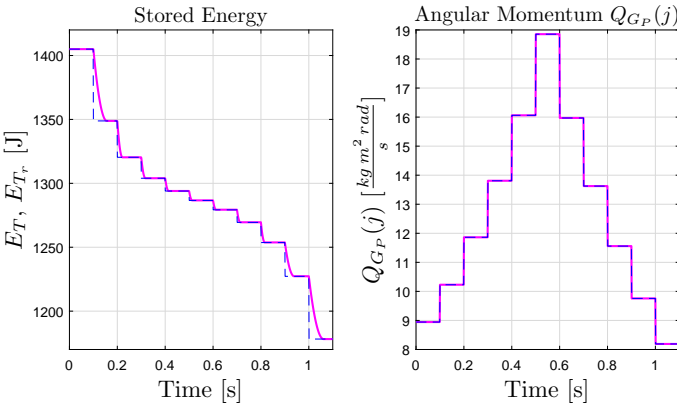Fig. 5. Angular velocities ω_p and ω_s; ratio α_{psj}.

Fig. 6. Energies E_T, E_{T_r}; angular momentum $Q_{G_P}(j)$.

gearbox model (blue line) simulations. The left subplot of Fig. 6 shows the total energies E_T (magenta line) and E_{T_r} (blue dashed line) vs time for the full (see Fig. 2) and reduced (see Fig. 3) models simulations, respectively. The corresponding expressions are:

$$E_T = \frac{1}{2} J_{T_p} \omega_p^2 + \frac{1}{2} J_{T_s} \omega_s^2, \qquad E_{T_r} = \frac{1}{2} J_T \omega_p^2.$$
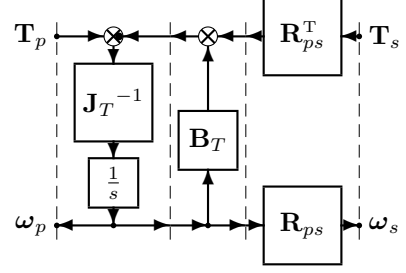

Fig. 7. Multidimensional version of the scheme in Fig. 3.

It can be noticed that an energy decrease occurs any time a gearshift takes place, lasting for a finite time in the simulation of the full gearbox model and occurring instantaneously in the simulation of the reduced gearbox model. This loss of energy is due to the action of the Coulomb friction torque between the primary and secondary shafts J_{T_p} and J_{T_s} in the full model of Fig. 2 during the synchronization phase. Note that the regime value (i.e. once the transient has ended) of the total energies E_T and E_{T_r} stored within the full and reduced models after gearshifting coincide, highlighting the correctness of the reduced gearbox dynamic model also from an energetic point of view. This can be achieved thanks to the fact that the new moment of inertia J_T after a gearshift, as well as the regime value of the primary shaft angular velocity ω_p after the synchronization phase, can be promptly computed thanks to (3) and (13), respectively. The right subplot of Fig. 6 shows the angular momentum $Q_{G_P}(j)$ defined in (4) for the full model simulation (magenta line) and for the reduced model simulation (blue dashed line). From the latter subplot, the reader can see that the two characteristics are indeed superimposed, as expected.

The saving in terms of simulation time of the reduced gearbox model with respect to the full model is around 17.66 %, also thanks to the fact that the reduced model of Fig. 3 does not require the usage of "sign" functions, thus reducing the computational load in the numerical simulation. This denotes the effectiveness and the compactness of the new reduced version of the gearbox dynamic model.

3. MULTIDIMENSIONAL CASE

This section analyzes the multidimensional case, where the primary and/or the secondary of the gearbox are connected to higher order systems. In such a case, the reduced gearbox model reported in Fig. 3 for the scalar case, i.e. one-dimensional dynamics both on the gearbox primary and on the gearbox secondary, can be generalized to the multidimensional version shown in Fig. 7. In the most general case, the primary is characterized by a dynamics of order n and the secondary is characterized by a dynamics of order m, with $n \geq 1$ and $m \geq 1$. Therefore, vectors and matrices present in the scheme of Fig. 7 have the following dimensions:

$$\mathbf{T}_p, \boldsymbol{\omega}_p \in {}^{(n \times 1)}, \qquad \mathbf{T}_s, \boldsymbol{\omega}_s \in {}^{(m \times 1)},$$

$$\mathbf{J}_T, \mathbf{B}_T \in {}^{(n \times n)}, \qquad \mathbf{R}_{ps} \in {}^{(m \times n)}$$

The angular momentum $Q_{Gp}(j)$ defined in (4) becomes:

$$\mathbf{Q}_{Gp}(j) = \mathbf{J}_{Tp} \boldsymbol{\omega}_p + \mathbf{R}_{ps}(j)^{\mathrm{T}} \mathbf{J}_{Ts} \boldsymbol{\omega}_s \qquad (14)$$

Prop. 1 still holds, and Eq. (13) extends as follows:

$$\boldsymbol{\omega}_p(t_j) = (\mathbf{P})^{-1} \left(\mathbf{J}_{Tp} + \mathbf{R}_{ps}(j)^{\mathrm{T}} \mathbf{J}_{Ts} \mathbf{R}_{ps}(i) \right) \boldsymbol{\omega}_p(t_{ij}) \quad (15)$$

where $\mathbf{P} = \mathbf{J}_{T_p} + \mathbf{R}_{ps}(j)^{\mathrm{T}} J_{T_s} \mathbf{R}_{ps}(j)$. Matrices $\mathbf{J}_T$ and $\mathbf{B}_T$ in Fig. 7 can be extended from relations (3) as follows:

$$\mathbf{J}_T = \mathbf{J}_{T_p} + \mathbf{R}_{ps}^{\mathrm{T}}\mathbf{J}_{T_s}\mathbf{R}_{ps} \quad \mathbf{B}_T = \mathbf{b}_{T_p} + \mathbf{R}_{ps}^{\mathrm{T}}\mathbf{b}_{T_s}\mathbf{R}_{ps} \quad (16)$$

3.1 Planetary Gear

Let us consider the planetary gear shown in Fig. 8 on the left, whose equivalent POG block scheme is reported on the right. The state space equations are the following:
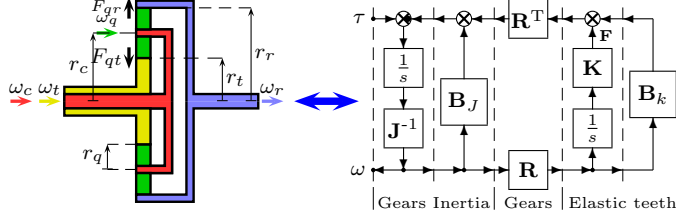

Fig. 8. Considered planetary gear: structure and model.

$$\begin{cases} \mathbf{L}\dot{\mathbf{x}} = \mathbf{A}\mathbf{x} + \mathbf{B}\mathbf{u}, \\ \mathbf{y} = \mathbf{B}^{\mathrm{T}}\mathbf{x} \end{cases}, \quad \mathbf{x} = \begin{bmatrix} \boldsymbol{\omega} \\ \mathbf{F} \end{bmatrix}, \quad \mathbf{u} = \boldsymbol{\tau}, \quad \mathbf{y} = \boldsymbol{\omega} \quad (17)$$

where matrices $\mathbf{L}$, $\mathbf{A}$ and $\mathbf{B}$ are defined in Zanasi and Tebaldi (2019), $\mathbf{F} = [F_{qt} \ F_{qr}]^{\mathrm{T}}$ and vectors $\boldsymbol{\omega}$ and $\boldsymbol{\tau}$ are:

$$\boldsymbol{\omega} = [\ \omega_c \ \ \omega_q \ \ \omega_t \ \ \omega_r\ ]^{\mathrm{T}} \qquad \boldsymbol{\tau} = [\ T_c \ \ T_q \ \ T_t \ \ T_r\ ]^{\mathrm{T}}\ .$$

Matrices $\mathbf{J}$, $\mathbf{B}_J$, $\mathbf{K}$ and $\mathbf{B}_K$ are defined as follows:

$$\mathbf{J} = \mathrm{diag}\,(J_c, J_q, J_t, J_r), \qquad \mathbf{B}_J = \mathrm{diag}\,(b_c, b_q, b_t, b_r)$$

$$\mathbf{K} = \mathrm{diag}\,(K_{qt}, K_{qr}), \qquad \mathbf{B}_K = \mathrm{diag}\,(b_{qt}, b_{qr})$$

Matrix $\mathbf{R}$, which fully and uniquely defines the model, see Zanasi and Tebaldi (2019), has the following structure:

$$\mathbf{R} = \begin{bmatrix} r_c & -r_q & -r_t & 0 \\ r_c & r_q & 0 & -r_r \end{bmatrix}.$$

If $\mathbf{K} \to \infty$, from (17) it follows $\mathbf{R}\,\boldsymbol{\omega} = 0$, giving the following congruent state space transformation:

$$\underbrace{\begin{bmatrix} \boldsymbol{\omega} \\ \mathbf{F} \end{bmatrix}}_{\mathbf{x}} = \underbrace{\begin{bmatrix} \mathbf{Q}_1 \\ \mathbf{0} \end{bmatrix}}_{\mathbf{T}_1} \underbrace{\begin{bmatrix} \omega_c \\ \omega_r \end{bmatrix}}_{\mathbf{x}_1} \Leftrightarrow \underbrace{\begin{bmatrix} \omega_c \\ \omega_q \\ \omega_t \\ \omega_r \\ F_{qt} \\ F_{qr} \end{bmatrix}}_{\mathbf{x}} = \underbrace{\begin{bmatrix} 1 & 0 \\ -\dfrac{r_c}{r_q} & \dfrac{r_r}{r_q} \\ \dfrac{2r_c}{r_t} & -\dfrac{r_r}{r_t} \\ 0 & 1 \\ 0 & 0 \\ 0 & 0 \end{bmatrix}}_{\mathbf{T}_1} \underbrace{\begin{bmatrix} \omega_c \\ \omega_r \end{bmatrix}}_{\mathbf{x}_1}$$

Applying $\mathbf{x} = \mathbf{T}_1\mathbf{x}_1$ to system (17), one obtains the following reduced model:

$$\underbrace{\begin{bmatrix} J_{1,1} & J_{1,2} \\ J_{1,2} & J_{2,2} \end{bmatrix}}_{\mathbf{L}_1} \underbrace{\begin{bmatrix} \dot{\omega}_c \\ \dot{\omega}_r \end{bmatrix}}_{\dot{\mathbf{x}}_1} = \underbrace{\begin{bmatrix} a_{1,1} & a_{1,2} \\ a_{1,2} & a_{2,2} \end{bmatrix}}_{\mathbf{A}_1} \underbrace{\begin{bmatrix} \omega_c \\ \omega_r \end{bmatrix}}_{\mathbf{x}_1} + \underbrace{\mathbf{Q}_1^{\mathrm{T}}}_{\mathbf{B}_1} \underbrace{\boldsymbol{\tau}}_{\mathbf{u}}. \quad (18)$$

The definition of matrices $\mathbf{L}_1$, $\mathbf{A}_1$ and $\mathbf{B}_1$ can be found in Zanasi and Tebaldi (2019).

3.2 Six Gearbox connected to a Planetary Gear

Let us consider the case reported in Fig. 9, showing the same gearbox as the one in Fig. 1 with the primary shaft rigidly connected to the ring of the planetary gear shown
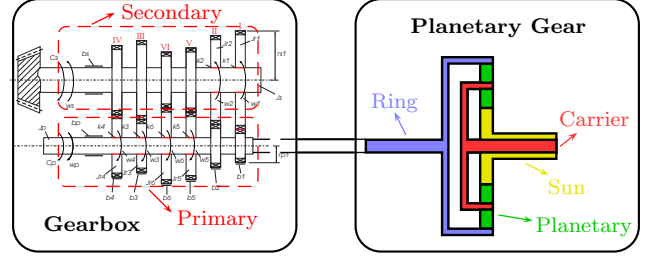

Fig. 9. Gearbox with primary shaft rigidly connected to the ring of a planetary gear.

Table 2. Parameters for simulation in Sec. 3.3.

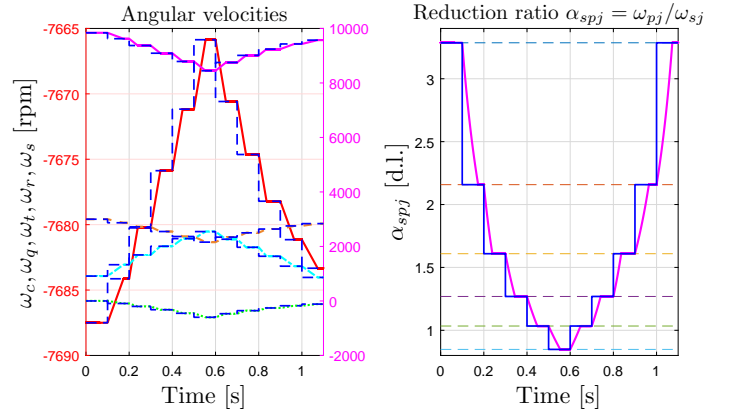|			
$J_c = 0.0198$,	$J_q = 0.0036$,	$J_t = 0.0038$	[kg m^2]
$J_r = 0.0842 + J_p + J_1\,\alpha_{ps1}^2 + J_2\,\alpha_{ps2}^2$			[kg m^2]
$b_c = 0$,	$b_q = b_c$,	$b_t = b_c$, $\quad b_r = b_c$	[(Nm s)/rad]
$r_c = 0.0855$,	$r_q = 0.0375$,	$r_t = 0.048$, $\quad r_r = 0.123$	[cm]

Fig. 10. Angular velocities; ratio α_{spj}.

in Fig. 8. This is the case of a multidimensional dynamics on the primary and a one-dimensional dynamics on the secondary, i.e. $n = 2$ (see system (18)) and $m = 1$. For the considered case study, the first component of vector $\mathbf{R}_{ps} \in {}^{(1\times 2)}$ is always equal to zero, because the carrier angular velocity ω_c does not influence the angular velocity ω_p of the primary shaft which is rigidly connected to the ring gear, see Fig. 9. The second component of vector $\mathbf{R}_{ps} \in {}^{(1\times 2)}$ is the reduction ratio α_{psj} defined in (2).

3.3 Multidimensional case study: simulation

In this section, the system in Fig. 9 is simulated using the full gearbox model in Fig. 2 extended to the multidimensional case and compared to the reduced multidimensional gearbox model shown in Fig. 7. The duration of the simulation T_{fin}, the initial angular velocity of the primary shaft (and thus of the ring gear) $\omega_{p_0} = \omega_{r_0}$ and the initial angular velocity of the secondary shaft ω_{s_0} are the same as those reported in Sec. 2.3 for the one-dimensional case. The initial carrier angular velocity is $\omega_{c_0} = 0$. The gearbox system parameters are the same as those reported in Table 1, expect for T_j, for $j \in [1,2,\ldots,6]$, which is equal to 50 [Nm]. The planetary gear parameters are those reported in Table 2. The engaged gear vs time is shown in Fig. 4, whereas Fig. 10 and Fig. 11 show the simulation results. The left subplot of Fig. 10 shows the time behavior of the angular velocities related to the primary dynamics: ω_c (green line), ω_q (magenta line), ω_t
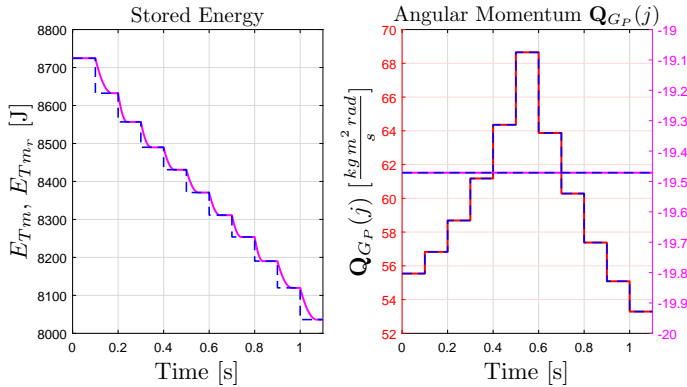
Fig. 11. Energies E_{Tm}, E_{Tm_r}; angular momentum $\mathbf{Q}_{G_P}(j)$.

(red line, with reference to left vertical axis), $\omega_r = \omega_p$ (orange line) and to the secondary dynamics ω_s (cyan line) for the simulation performed on the original full model described in Sec. 2.1 extended to the multidimensional case, as well as the corresponding angular velocities of the primary and secondary dynamics for the simulation performed on the reduced multidimensional model in Fig. 7 (blue dashed lines). The right subplot of Fig. 10 shows the reduction ratio α_{spj} for the simulation performed on the full gearbox model (magenta line) and on the reduced gearbox model (blue line). The left subplot of Fig. 11 shows the evolution of the total energies E_{Tm} (magenta line) and E_{Tm_r} (blue dashed line) during the simulation performed on the full and reduced gearbox multidimensional models, respectively. The corresponding expressions are:

$$E_{Tm} = \frac{1}{2} \begin{bmatrix} \omega_c & \omega_r \end{bmatrix} \mathbf{J}_{T_p} \begin{bmatrix} \omega_c \\ \omega_r \end{bmatrix} + \frac{1}{2} J_{T_s} \omega_s^2,$$

$$E_{Tm_r} = \frac{1}{2} \begin{bmatrix} \omega_c & \omega_r \end{bmatrix} \mathbf{J}_T \begin{bmatrix} \omega_c \\ \omega_r \end{bmatrix}.$$

Similar considerations as those made for Fig. 6-left subplot can be made for Fig. 11-left subplot, highlighting the energetic correctness of the reduced model. The right subplot of Fig. 11 shows the first component of the angular momentum $\mathbf{Q}_{G_P}(j)$ in (14) reported on the primary for the simulation on the full gearbox multidimensional model (magenta line) and for the simulation on the reduced gearbox multidimensional model in Fig. 7 (blue dashed line) with reference to the right vertical axis. Additionally, the right subplot of Fig. 11 shows the second component of the angular momentum $\mathbf{Q}_{G_P}(j)$ in (14) reported on the primary for the simulation on the full gearbox multidimensional model (red line) and on the reduced gearbox multidimensional model in Fig. 7 (blue dashed line) with reference to the left vertical axis. From this subplot, the reader can notice that the only component of $\mathbf{Q}_{G_P}(j)$ which is affected by a gear shifting is the second one, i.e. the one affected by the variation of vector $\mathbf{R}_{ps}$ when a gearshift occurs, as the first component of $\mathbf{R}_{ps}$ in (14) is equal to zero for the considered case study.

The saving in terms of simulation time of the reduced gearbox model with respect to the full model in the multi-dimensional case is around 9.09 %, also thanks to the fact that the reduced multidimensional model of Fig. 7 does not require the usage of "sign" functions, thus reducing the computational load in the numerical simulation. This

once again denotes the effectiveness and the compactness of the new reduced version of the gearbox dynamic model.

4. CONCLUSIONS

In this paper, a new gearbox dynamic model for the simulation of simultaneous multi-clutches lock/unlock has been presented. The model exploits the conservation of the angular momentum defined in a determined point of the system even during the gear engagement phase. From the latter angular momentum, the new shafts velocities can be instantaneously determined by skipping the transient, thus reducing the computational complexity of the simulation, while preserving the natural energy loss associated to gear shifting. This new approach has been applied to two case studies, the second one foreseeing a multidimensional primary dynamics for the gearbox system. Simulation results have been provided for both case studies, showing the effectiveness of the presented approach.

REFERENCES

M. Bachinger, M. Stolz, M. Horn. Fixed Step Clutch Modeling and Simulation for Automotive Real-Time Applications. Proceedings of the American Control Conference (ACC), 4-6 June 2014.

F. Grossi, R. Zanasi. Dynamic Modeling of a Double Clutch for Real-Time Simulations. Proceedings of the European Control Conference (ECC), 15-17 July 2015.

W. Lhomme, R. Trigui, A. Bouscayrol, P. Delarue, B. Jeanneret, F. Badin. Validation of Mechanical Transmission with Clutch using Hardware-In-the-Loop Simulation. Proceedings of the IEEE Vehicle Power and Propulsion Conference (VPPC), 9-12 Sept. 2007.

Xian-an SUN, Guang-qiang WU, Lin HE Guo-ling KONG. Hardware-in-the-loop Simulation for Electro-control System of Continuously Variable Transmission Based on DSPACE. Proceedings of the IEEE Vehicle Power and Propulsion Conference (VPPC), 3-5 Sept. 2008.

R. Zanasi. The Power-Oriented Graphs technique: System modeling and basic properties. Proceedings of the IEEE Vehicle Power and Propulsion Conference (VPPC), 1-3 Sept. 2010.

R. Zanasi, F. Grossi. The POG Technique for Modeling Planetary Gears and Hybrid Automotive Systems. Proceedings of the IEEE Vehicle Power and Propulsion Conference (VPPC), 7-11 Sept. 2009.

R. Zanasi, G. Sandoni, A. Visconti "Dynamin Model and Control of a Gearbox System", Mechatronics 2002, Twente, Enschede, Netherlands, June 24-26 2002.

R. Zanasi, D. Tebaldi. Planetary Gear Modeling Using the Power-Oriented Graphs Technique. Proceedings of the European Control Conference (ECC), 25-28 June 2019.

R. Zanasi, A. Visconti, G. Sandoni, R. Morselli. Dynamic Modeling and Control of a Car Transmission System. Proceedings of the International Conference on Advanced Intelligent Mechatronics (AIM), 8-12 July 2001.

M. Zoppi, C. Cervone, G. Tiso, F. Vasca. Software in the loop model and decoupling control for dual clutch automotive transmissions. Proceedings of the 3rd International Conference on Systems and Control (ICSC), 29-31 Oct. 2013.